molecules

MDPI

Article

Synthesis and Anticancer Evaluation of PCNA Inhibitor AOH1996 Analogs in Cancer Cell Cultures

Simona Jonušienė [1,*], Agnė Janonienė [2], Mantas Jonušis [3], Adas Darinskas [4] and Denis Sokol [1]

[1] Faculty of Chemistry and Geosciences, Institute of Chemistry, Vilnius University, Naugarduko g. 24, LT-03225 Vilnius, Lithuania; denis.sokol@chgf.vu.lt
[2] Life Sciences Center, Institute of Biotechnology, Vilnius University, Saulėtekio g. 7, LT-10257 Vilnius, Lithuania; agne.vegyte@bti.vu.lt
[3] Life Sciences Center, Institute of Biochemistry, Vilnius University, Mokslininkų g. 12A, LT-08412 Vilnius, Lithuania; mantas.jonusis@gmc.vu.lt
[4] Laboratory of Immunology, National Cancer Institute, P. Baublio g. 3b, LT-08406 Vilnius, Lithuania; darinskas.adas@gmail.com
* Correspondence: simona.jonusiene@gmc.vu.lt

Abstract

Proliferating cell nuclear antigen (PCNA) is a critical regulator of DNA replication and repair, and its cancer-associated isoforms represent promising therapeutic targets. The small molecule AOH1996 has been previously reported as a PCNA inhibitor with potent antiproliferative activity. Here, a series of novel AOH1996-based structural analogs were synthesized using structure–activity relationship (SAR) and scaffold-hopping strategies, including 1,2,3-triazole, glycine, and amide derivatives with diverse aromatic and polar substituents. The antiproliferative activity of these compounds was evaluated in MCF-7 (breast cancer) and U87 (glioblastoma) cell lines using the MTT assay. The parent compound AOH1996 exhibited the strongest cytotoxicity, reducing cell viability below 30% at 10 μM. Among the analogs, compounds **1f**, **2b**, **3b**, **3c**, and **3d** demonstrated significant activity, reducing MCF-7 viability by 60–70% and U87 viability to 30–40% at 10 μM. SAR analysis revealed that electron-withdrawing or moderately lipophilic substituents on the amide side chain and aromatic extensions on the triazole ring enhanced potency, while bulky or strongly electron-donating groups diminished activity. ADMET predictions indicated that most derivatives possessed favorable drug likeness and absorption potential, but high plasma protein binding, short predicted half-lives, and potential cardiotoxicity represent limitations that will require further optimization. Several active compounds were predicted to inhibit P-glycoprotein, suggesting their potential to overcome multidrug resistance. Overall, compounds **2b** and **3b** showed relatively favorable predicted profiles and can serve as useful lead scaffolds for further optimization and experimental validation.

Keywords: PCNA inhibitor; AOH1996 analogs; structure–activity relationship; anticancer activity; MCF-7; U87; cytotoxicity; ADMET prediction

Academic Editor: Chiara Brullo

Received: 13 February 2026
Revised: 1 March 2026
Accepted: 3 March 2026
Published: 5 March 2026

1. Introduction

Proliferating cell nuclear antigen (PCNA) is an important protein in DNA replication, repair, chromatin organization, and cell cycle regulation, making it essential for the proliferation and survival of both normal and cancer cells [1]. PCNA is a homotrimeric ring-shaped protein that encircles DNA and acts as a sliding clamp, recruiting DNA polymerases and repair proteins via specific motifs (PIP-box, APIM) that bind to its hydrophobic pocket.

Inhibition of PCNA can occur through several mechanisms, each targeting its central role in DNA metabolism (Table 1).

Table 1. Summary of PCNA inhibition mechanisms and their biological effects.

Inhibitor Type	Mechanism of Action	Biological Consequence
Small molecules (e.g., T2AA)	Block PIP-box/monoubiquitinated PCNA interactions	Inhibit TLS, impair DNA repair, sensitize to chemotherapy
Peptides (PIP-box/APIM mimics)	Compete for PCNA binding pocket	Disrupt replication/repair protein recruitment
Aptamers	Form stable complexes with PCNA and DNA polymerases	Block DNA synthesis at replication fork
Endogenous proteins (p21)	Bind PCNA, block polymerase activation	Inhibit DNA replication, cell cycle arrest
Genetic/pharmacologic inhibition	Disrupt PCNA-PARP1 axis, impair DNA repair/cell cycle progression	Sensitize PARP inhibitors, induce apoptosis

PCNA in cancer cells is frequently overexpressed, correlating with aggressive tumor behavior, poor prognosis, and resistance to therapy, thus establishing it as a promising biomarker and therapeutic target. Historically, PCNA was considered "undruggable" owing to its lack of deep binding pockets and the absence of endogenous small-molecule modulators, but recent advances in structural biology and drug discovery have led to the identification of small molecules and peptides capable of disrupting PCNA function [2]. Overexpression and cancer-specific isoforms of PCNA (notably, caPCNA) are associated with aggressive tumor phenotypes and poor treatment prognosis across multiple cancer types, including hepatocellular carcinoma, glioblastoma, pancreatic ductal adenocarcinoma, multiple myeloma, and others [3–7].

Small molecules, peptides, or aptamers can bind to the hydrophobic pocket of PCNA—often at the interdomain connecting loop or the PIP-box binding site—thereby preventing the association of PCNA with its protein partners, such as DNA polymerases δ and ε, or repair factors like p15 and PARP1. For example, anti-PCNA aptamers can form stable complexes with PCNA and DNA polymerases, outcompeting primer-template DNA and directly blocking the assembly of the replication machinery, which halts DNA synthesis at the replication fork [8,9]. Small-molecule inhibitors like T2AA specifically disrupt interactions between monoubiquitinated PCNA and translation synthesis (TLS) polymerases (e.g., pol η, REV1), impairing the repair of interstrand DNA cross-links and enhancing DNA double-strand breaks, especially in the presence of DNA-damaging agents such as cisplatin [10]. Peptidic inhibitors, such as those mimicking the PIP-box or APIM motifs, competitively inhibit the binding of PCNA to its partners, thereby suppressing DNA replication and repair processes and sensitizing tumor cells to genotoxic stress. Additionally, endogenous inhibitors like the C-terminal domain of p21 can bind PCNA and block its ability to activate DNA polymerase δ, leading to cell cycle arrest independent of cyclin-dependent kinase inhibition [11]. PCNA inhibition also disrupts its interaction with PARP1, a key player in the DNA damage response, further impairing DNA repair and promoting cell cycle arrest or apoptosis in cancer cells. Collectively, these mechanisms converge on the disruption of PCNA's scaffolding function, leading to impaired DNA synthesis, defective repair, cell cycle blockade, and increased sensitivity to DNA-damaging therapies, making PCNA a promising target for cancer treatment.

Notable examples of small-molecule inhibitors of PCNA include T2 amino alcohol S-T2AA, AOH1996, PCNA-I1, LRRK2-IN-1, SAR-24, and T2AA-NEal-NTyr, each with distinct mechanisms and selectivity profiles (Figure 1) [2,10].

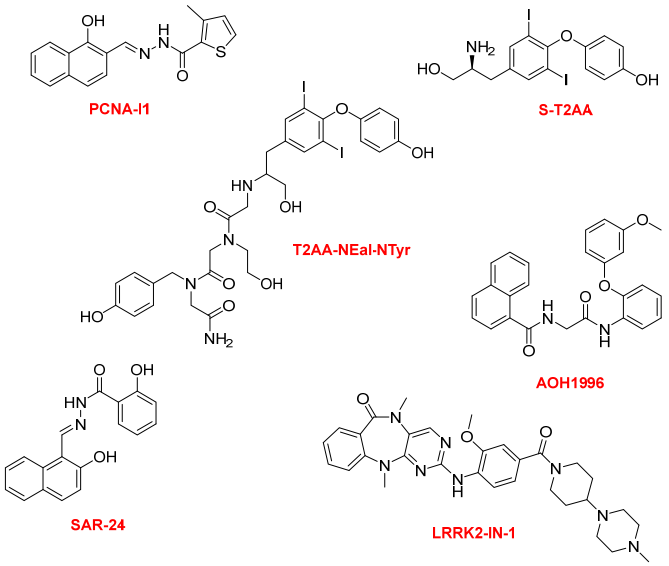

Figure 1. Examples of small-molecule PCNA inhibitors.

T2AA and its analogs inhibit PCNA/PIP-box interactions, leading to DNA replication stress and chemosensitization. AOH1996, a first in its class inhibitor, selectively targets a cancer-associated PCNA isoform (caPCNA). The development of small-molecule PCNA inhibitors, particularly AOH1996, represents a breakthrough in targeted cancer therapy. Notably, the small molecule AOH1996 has emerged as a leading candidate, demonstrating the ability to bind caPCNA, stabilize its trimeric structure, and disrupt its association with chromatin, thereby selectively inducing cancer cell death without affecting non-cancerous cells. AOH1996 and its analogs, developed through structure–activity relationship (SAR) studies and scaffold-hopping strategies, have shown enhanced potency, selectivity, and metabolic stability, with some analogs exhibiting up to nine-fold improved efficacy and increased liver microsome stability. These compounds are now in phase 1 clinical trials [12]. AOH1996 is designed to selectively bind to a cancer-associated region of PCNA, disrupting its interactions with key proteins involved in DNA replication, repair, and transcription–replication conflict resolution [4,12–16]. AOH1996 also exhibits anti-metastatic properties by inhibiting angiogenesis, cancer cell migration, and modulating the tumor microenvironment, including suppression of MYC expression and tumor-associated macrophage recruitment. Furthermore, AOH1996 shows promise in combination therapies, including with histone deacetylase inhibitors, KRAS inhibitors, platinum agents, and PARP inhibitors. These advances underscore the growing importance of PCNA inhibitors, and especially AOH1996, as innovative and potentially transformative agents in the fight against cancer.

Researchers have conducted extensive structure–activity relationship (SAR) studies, synthesizing more than 100 analogs by systematically altering three core structural elements: the naphthyl group, glycine linker, and the diphenyl ether segment (Figure 2).

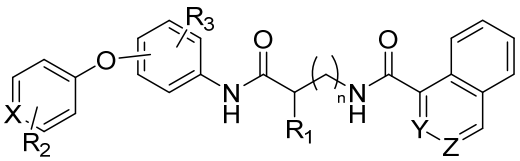

Figure 2. Core structure of known studied analogs of AOH1996.

These modifications included replacing the glycine linker with various amino acids, substituting the 1-naphthoyl group with alternative aromatic systems like quinoline and isoquinoline, and introducing a range of functional groups—such as sulfonyl, imido, sulfur,

amide, halogen, or methyl groups—at different positions on the diphenyl ether. Through these strategies, analogs like AOH1160S, AOH1996S-4CH3, and AOH1996-3CH3 were identified, exhibiting equal to or greater potency than the original compound. Additional approaches, including scaffold-hopping and bioisostere replacement, produced analogs with unsymmetrical 3-methoxy-5-methyl groups and further substitutions, resulting in up to nine-fold increased potency and markedly improved metabolic stability [2].

Our scientific group synthesized a series of compounds in which the structure is based on the AOH-1996 scaffold, designed with the expectation that they could potentially modulate PCNA-associated pathways. Here, we investigate their anticancer properties in MCF-7 and U87 cell cultures and ADMET predictions of various glycine derivatives, including *N*-substituted glycine derivatives, triazoles formed from intermediate azides and various terminal acetylenes, and compounds with substituents other than naphthoyl and attached strained heterocycles such as aziridine and azetidine.

2. Results and Discussion

To start with, modeling of the AOH1996 interaction with PCNA involved detailed structural studies, including crystallography of PCNA in complex with AOH1996 and its more soluble analogs, confirming binding at the PIP box cavity and adjacent pockets critical for protein–protein interactions. Scaffold-hopping and bioisostere replacement strategies further enhanced potency, selectivity, and metabolic stability, leading to analogs such as AOH-3M5Me-6F and AOH-3M5Me-6CN, which demonstrated up to nine-fold improved potency and greater liver microsome stability compared to the clinical lead [17]. Synthesis of these inhibitors typically involved combinatorial chemistry approaches, such as fragment-based design and flexible *N*-alkyl-glycine amide scaffolds, enabling the exploration of diverse subpockets on PCNA and the rapid generation of compound libraries for screening [18]. Following the evaluation of the established PCNA inhibitor AOH1996 for its anticancer efficacy in cell models and informed by findings from prior studies, we initiated the synthesis of novel, previously unreported potential PCNA inhibitors. Structural modifications were guided by structure–activity relationship (SAR) analyses and scaffold-hopping strategies, incorporating both alterations described in the literature and original modifications developed in this work. Figure 2 presents an overview of the structural changes introduced by other researchers [2], alongside the novel modifications to the core scaffold described herein (Scheme 1).

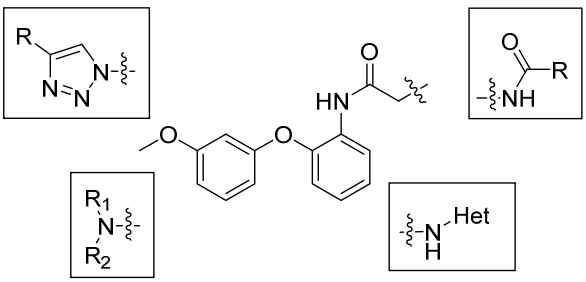

Scheme 1. Novel modifications to the core scaffold described herein.

A series of 4-substituted 1,2,3-triazole derivatives (compounds **1a**–**g**) was synthesized using the copper(I)-catalyzed azide–alkyne cycloaddition (CuAAC) reaction. The synthesis involved the reaction of substituted organic azide with various terminal alkynes, as depicted in Scheme 2. The CuAAC reaction proceeded regiospecifically to afford 1,4-disubstituted triazoles, with copper(I) facilitating cycloaddition between the azide and alkyne components under mild conditions. Reactions were performed strictly under an inert argon atmosphere to prevent oxidation of Cu(I) to Cu(II) (Scheme 2) (Table 2).

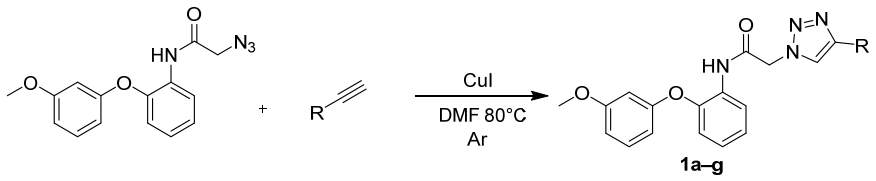

Scheme 2. Synthesis scheme for compounds **1a**–**g**.

Table 2. Assignment of R groups to compounds **1a**–**g**.

Compound	R
1a	$ClCH_2CH_2CH_2$
1b	Ph
1c	4-F-Ph
1d	4-OMe-Ph
1e	4-Et-Ph
1f	4-Ph-Ph
1g	4-*n*-Amyl-Ph

Also, a series of derivatives, designated as compounds **2a**–**g**, were synthesized via nucleophilic substitution of the 2-chloroacetamide derivative with a range of cyclic and acyclic amines, including aziridine, azetidine, pyrrolidine, etc. (Scheme 3) (Table 3). Reactions were performed in refluxing acetonitrile using excess of amine.

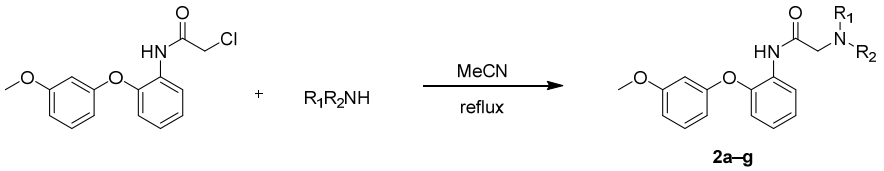

Scheme 3. Synthesis scheme for compounds **2a**–**g**.

Table 3. Assignment of R groups to compounds **2a**–**g**.

Compound	R_1	R_2
2a	Me	Me
2b	CH_2CH_2	
2c	$(CH_2)_3$	
2d	Me	Bn
2e	$(CH_2)_4$	
2f	$(CH_2)_5$	
2g	$O(CH_2CH_2)_2$	

The parent compound, 2-amino-*N*-(2-(3-methoxyphenoxy)phenyl)acetamide, exhibited no observable anticancer activity in all preliminary assays. Consequently, a new series of derivatives was synthesized by functionalizing the initial acetamide scaffold with variously substituted benzoyl chlorides, cyanuric chloride, and 3,6-dichloro-1,2,4,5-tetrazine, in an effort to enhance potential anticancer properties (Scheme 4) (Table 4).

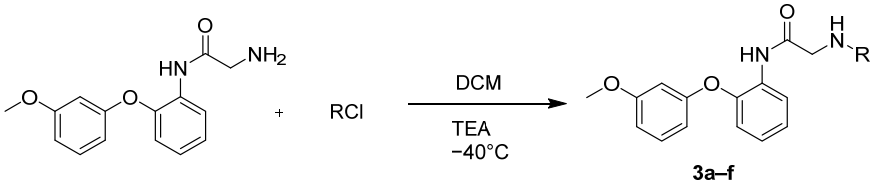

Scheme 4. Synthesis scheme for compounds **3a**–**f**.

Table 4. Assignment of R groups to compounds **3a**–**f**.

Compound	R
3a	4-NO_2PhCO
3b	2-FPhCO
3c	2-ClPhCO
3d	Ph$(CH_2)_3$CO
3e	4,6-dichloro-1,3,5-triazin-2-yl
3f	6-chloro-1,2,4,5-tetrazin-3-yl

Moreover, the cytotoxic activity of the synthesized AOH1996 derivatives was assessed in MCF-7 (breast cancer) and U-87 (glioblastoma) cell lines after 72 h of treatment using the MTT assay (Table 5). The parent compound AOH1996 exhibited the strongest antiproliferative effect, reducing cell viability to below 30% at a concentration of 10 μM in both cell lines. Among the derivatives, compounds **1f**, **2b**, **3b**, **3c**, and **3d** showed significant reductions in cell viability. Compounds **1f**, **3b**, **3c**, and **3d** at a concentration of 10 μM reduced MCF-7 cell viability by 60–70% and demonstrated the highest activity within the series. In the U-87 cell line, compounds **1f**, **2b**, **3b**, and **3c** at a concentration of 10 μM reduced cell viability to 30–40%. Derivatives **1a**, **2f**, **2g**, **3a**, and **3e**, however, maintained a cell viability above 70% across both cell lines at a concentration of 10 μM, indicating limited antiproliferative effects. These results suggested that the incorporation of electron-withdrawing or moderately lipophilic substituents enhanced the cytotoxic potency of the AOH1996 scaffold, whereas bulky or strongly electron-donating groups diminished activity.

Table 5. Cytotoxicity screening of AOH1996 and its derivatives against MCF-7 and U-87 cancer cell lines and BJ-5ta non-cancer cell line after 72 h treatment.

Compound	Concentration (μM)	Cell Viability (% ± SD)			SI (BJ-5ta)	
		MCF-7	U-87	BJ-5ta	vs. MCF-7	vs. U-87
1a	10	88.9 ± 5.6	68.5 ± 2.0	72.4 ± 1.8	<2	<2
	100	13.8 ± 6.5	23.5 ± 1.1	20.2 ± 4.4	<2	<2
1f	1	72.1 ± 1.0	70.2 ± 9.0	97.7 ± 7.0	<2	<2
	10	41.2 ± 9.6	28.2 ± 5.2	83.5 ± 4.0	≥2	≥2
	100	9.2 ± 0.4	12.8 ± 1.5	56.9 ± 4.1	≥2	≥2
2b	1	63.2 ± 9.1	74.5 ± 5.4	96.3 ± 7.5	<2	<2
	10	59.1 ± 5.7	41.0 ± 2.5	73.6 ± 5.6	<2	<2
	100	4.9 ± 1.0	13.3 ± 2.1	18.2 ± 3.1	≥2	<2
2f	10	89.6 ± 3.7	82.1 ± 5.3	84.9 ± 11.1	<2	<2
	100	4.7 ± 0.2	26.3 ± 4.0	52.0 ± 6.8	≥2	≥2
2g	10	89.9 ± 5.6	88.3 ± 6.1	98.7 ± 8.0	<2	<2
	100	20.7 ± 6.5	78.3 ± 1.1	73.1 ± 5.1	≥2	<2
3a	1	93.0 ± 3.8	64.1 ± 11.1	93.5 ± 4.5	<2	<2
	10	65.3 ± 1.9	62.0 ± 12.2	82.1 ± 7.9	<2	<2
	100	26.4 ± 0.4	45.5 ± 3.9	74.2 ± 5.6	≥2	<2
3b	1	77.3 ± 4.1	50.0 ± 10.3	89.3 ± 6.0	<2	<2
	10	42.1 ± 2.9	36.7 ± 10.4	70.7 ± 2.3	<2	<2
	100	9.2 ± 1.5	23.8 ± 2.4	38.7 ± 3.5	≥2	<2
3c	1	50.3 ± 6.0	59.2 ± 2.1	78.6 ± 3.5	<2	<2
	10	28.8 ± 6.5	38.7 ± 5.3	31.0 ± 3.5	<2	<2
	100	6.6 ± 0.2	16.1 ± 3.5	38.5 ± 8.8	≥2	≥2
3d	1	62.0 ± 8.0	55.9 ± 3.2	95.0 ± 4.6	<2	<2
	10	44.5 ± 4.6	54.5 ± 3.2	88.6 ± 0.6	≥2	<2
	100	29.0 ± 10.3	56.2 ± 3.5	37.2 ± 3.6	<2	<2

Table 5. *Cont.*

Compound	Concentration (μM)	Cell Viability (% ± SD)			SI (BJ-5ta)	
		MCF-7	U-87	BJ-5ta	vs. MCF-7	vs. U-87
3e	10	93.8 ± 2.4	99.1 ± 8.9	94.6 ± 9.3	<2	<2
	100	6.2 ± 0.1	93.0 ± 4.3	80.5 ± 6.1	≥2	<2
AOH1996	1	40.5 ± 10.2	43.4 ± 12.9	54.2 ± 6.8	<2	<2
	10	17.9 ± 8.4	25.9 ± 2.0	46.7 ± 4.7	≥2	<2
	100	12.9 ± 0.8	21.2 ± 2.0	36.1 ± 3.8	≥2	<2

Cells were treated with compounds at 1, 10, and 100 μM. Viability was determined using the MTT assay and expressed as a percentage of vehicle-treated control (DMSO, 100% viability). Data represent the mean ± standard deviation (SD) from three independent experiments performed in triplicate. The Selectivity Index (SI) was calculated as the ratio of % viability in BJ-5ta normal fibroblasts to % viability in cancer cells (MCF-7 or U-87) at the same concentration.

Importantly, evaluation in a non-cancerous cell line (BJ-5ta) demonstrated reduced cytotoxic effects for the majority of derivatives.

Based on the preliminary screening, six compounds (**1f**, **2b**, **3b**, **3c**, **3d**, and parent AOH1996) were selected for full dose–response analysis. As shown in Figure 3, distinct cell line-dependent activity profiles were observed. In MCF-7 breast cancer cells, several derivatives showed similar potency (**3b** IC_{50} = 0.93 μM, **3c** IC_{50} = 0.85 μM, **3d** IC_{50} = 0.93 μM) to AOH1996 (IC_{50} = 1.74 μM). By contrast, in U-87 glioblastoma cells, AOH1996 remained the most potent compound (IC_{50} = 0.99 μM), with all derivatives showing lower potency (IC_{50} 8.72–38.50 μM) relative to the parent compound. Among the derivatives, **3d** retained the highest activity in this cell line.

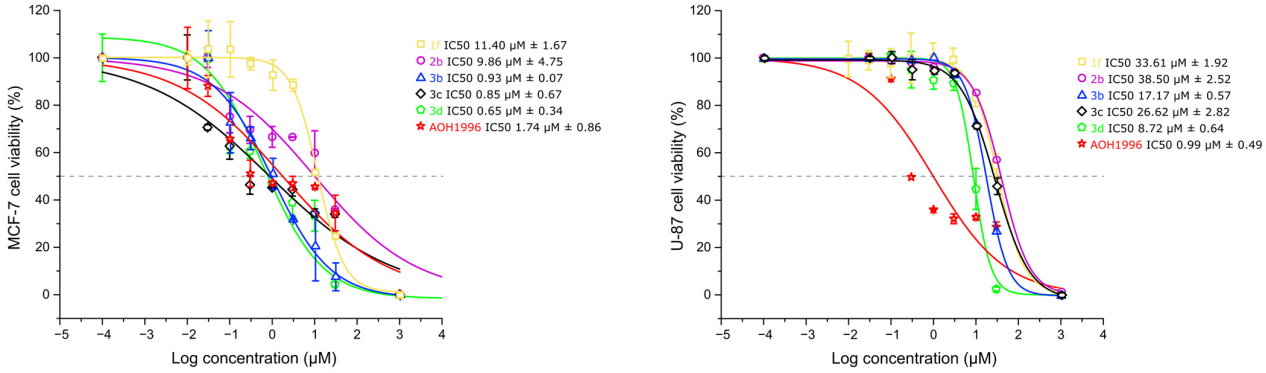

Figure 3. Dose response curves and calculated IC_{50} values of selected AOH1996 derivatives and the parent compound in MCF-7 and U87 cell lines after 72 h of treatment. Cell viability was determined using the MTT assay and expressed as a percentage relative to vehicle treated controls. Different colored lines represent distinct compounds, as indicated in the legend. The horizontal dashed line marks 50% cell viability, corresponding to the IC_{50} threshold.

Structure—Activity Relationship

The SAR analysis of the AOH1996 derivatives indicated that compounds **1f**, **2b**, **3b**, **3c**, and **3d** exhibited the most pronounced antiproliferative activity, suggesting that specific structural features on both the triazole and amide moieties played key roles in modulating potency. Compound **1f**, containing a benzyl-substituted triazole, demonstrated notable cytotoxicity, likely due to enhanced π–π interactions and increased lipophilicity, which facilitated membrane penetration. The aziridine-bearing derivative **2b** also showed good activity, suggesting that small polar rings could significantly improve reactivity and possibly favor target binding through hydrogen-bond interactions. Among the **3**-series derivatives, the presence of electron-withdrawing substituents such as fluoro (**3b**) and chloro (**3c**) groups, as well as the phenylalkyl chain (**3d**), significantly improved antiproliferative

effects, consistent with improved electronic complementarity and optimal lipophilicity for cellular uptake. Comparison of activity in cancerous versus non-cancerous cells suggested that increased lipophilicity alone did not directly correlate with nonspecific toxicity. Derivatives such as **1f** and **3d** appeared to achieve improved cancer cell selectivity. By contrast, derivatives with bulky or strongly electron-donating groups (e.g., **1a**, **2f**, **2g**, **3a**, and **3e**) displayed reduced anticancer activity, likely due to steric hindrance or an altered physicochemical balance that compromised target affinity or permeability. Overall, these results highlighted that moderate lipophilicity combined with electron-withdrawing substituents on the amide side chain and aromatic extensions on the triazole ring enhanced anticancer potency, making compounds **1f**, **2b**, **3b**, **3c**, and **3d** the most promising scaffolds for further optimization.

3. Materials and Methods

3.1. Cell Culturing

Human breast cancer cell line MCF-7 (ATCC HTB-22^{TM}) and human glioblastoma cell line U87 (ATCC HTB-14^{TM}) were used in the experiments. These cell lines were selected as representative models of highly proliferative solid tumors in which PCNA is overexpressed and associated with tumor progression and poor prognosis [19,20]. MCF-7 is a well-characterized, hormone-responsive breast cancer model widely used in antiproliferative screening studies, whereas U87 is an aggressive glioblastoma model with high replicative activity and therapeutic resistance, and is commonly used to test novel compounds. Human foreskin fibroblast BJ-5ta (ATCC CRL-4001^{TM}) was used as a non-cancerous control cell line to assess selectivity. Cells were cultured in Dulbecco's modified Eagle medium (DMEM, Gibco, Grand Island, NY, USA) supplemented with 10% fetal bovine serum (FBS, Gibco, Grand Island, NY, USA) and 1% penicillin/streptomycin (Gibco, Grand Island, NY, USA). Cell cultures were maintained in a humidified incubator at 37 °C with 5% CO_2.

The human breast cancer cell line MCF-7 (ATCC HTB-22™) and the human glioblastoma cell line U87 (ATCC HTB-14™) were originally obtained from the American Type Culture Collection (ATCC, Manassas, VA, USA) and kindly provided by Prof. Daumantas Matulis (Vilnius University, Vilnius, Lithuania). Human foreskin fibroblasts BJ-5ta (ATCC CRL-4001™) were also originally obtained from ATCC and kindly provided by Prof. Helder Santos (University of Helsinki, Helsinki, Finland).

3.2. MTT Cell Viability Assay

The antiproliferative influence of the compounds was determined using the MTT assay, which measures the activity of mitochondrial dehydrogenases in metabolically active cells. Cells were seeded in 96-well plates (TPP, Trasadingen, Switzerland) at a density of 10,000 cells per well and allowed to adhere overnight. The medium was then aspirated and replaced with fresh medium containing the test compounds. Compounds were prepared by serial dilution from stock solutions (50 mM in DMSO; Fisher Scientific, Waltham, MA, USA), ensuring the final concentration of DMSO in all wells did not exceed 0.2% (v/v). Control wells included a negative control (medium with 0.2% DMSO, serving as the vehicle control) and a positive control (medium with 1% Triton X-100; Fisher Scientific, Waltham, MA, USA). The plates were incubated for 72 h. Following the 72 h treatment, 10 µL of 5 mg/mL MTT (Invitrogen, Thermo Fisher Scientific, Waltham, MA, USA) solution in phosphate-buffered saline (PBS; Gibco, Grand Island, NY, USA) was added to each well, and the plates were incubated for an additional 4 h to allow for formazan crystal formation. The medium was then carefully removed, and 100 µL of DMSO was added to each well to dissolve the resulting formazan crystals. The absorbance was measured at 570 nm using a microplate reader (CLARIOstar Plus; BMG LABTECH, Ortenberg, Germany), with a 650 nm reference

wavelength employed to account for background absorbance. Cell viability was calculated as a percentage relative to the vehicle control.

The IC_{50} values were determined from dose–response curves fitted using a four-parameter logistic nonlinear regression model in Origin 2015 software (OriginLab, Northampton, MA, USA) with eight concentrations of the compounds (0.01–30 μM). IC_{50} values are reported as the mean ± SD. All measurements were repeated at least three times.

3.3. Predicted ADMET Properties

Cell viability was calculated as a percentage of the vehicle-treated control (0.2% DMSO). All experiments were performed in triplicate and repeated at least three times. Dose–response graphs were generated (Figure 3). Data are presented as the mean ± standard deviation.

ADMET properties, including absorption, distribution, metabolism, excretion, and toxicity parameters, were predicted using the ADMETlab 3.0 online platform (https://admetmesh.scbdd.com/, accessed on 1 September 2025) based on structure-input analysis [21].

The medicinal chemistry profiles predicted by ADMETlab 3.0 indicated that all compounds satisfied the Lipinski, Pfizer, and Golden Triangle rules, suggesting acceptable drug likeness. However, the GSK rule (MW $\leq$ 400; logP $\leq$ 4) was satisfied only for compounds **2b** and **3b**, while others exceeded the molecular weight threshold.

The Human Intestinal Absorption (HIA) predictions indicated generally high intestinal absorption for compounds (predicted values $\geq$ 30% for all derivatives) and the potential for good oral bioavailability. The predicted Caco-2 permeability values for all derivatives further supported favorable membrane permeability and consistent absorption potential across the series. Evaluation of P-glycoprotein (P-gp) interactions showed that compounds **2b**, **3b**, and **3d** had high or moderate probabilities of being P-gp inhibitors, which could help to overcome multidrug resistance in tumor cells, although the clinical relevance remains to be verified experimentally. The predicted plasma protein binding (PPB) was approximately 98% for all compounds. Such high PPB values are generally unfavorable, as they may result in lower free drug concentrations and a reduced therapeutic index. The volume of distribution (VDss) values were within the optimal range (0.04–20 L/kg) for compounds **1f** and **2b**. Blood–brain barrier (BBB) permeability predictions, relevant to CNS-targeted therapy (e.g., glioblastoma), indicated that compound **3c** had the highest probability of BBB penetration, while compound **2b** showed a low probability, suggesting limited CNS exposure.

ADMETlab 3.0 predicted that compounds **2b** and **3d** were likely CYP3A4 and CYP2D6 inhibitors and substrates, showing high probabilities of enzyme interaction and poor metabolic stability (HLM > 0.99), highlighting the potential for rapid hepatic metabolism and drug–drug interactions. This suggested rapid hepatic metabolism and a higher potential for drug–drug interactions. By contrast, compounds **1f**, **3c**, and **3b** displayed low CYP interaction probabilities and lower HLM instability values (<0.3), indicating favorable metabolic stability and a lower likelihood of CYP-mediated metabolism. Regarding elimination kinetics, all compounds except **1f** showed moderate plasma clearance (5–15 mL/min/kg), while compound **1f** exhibited low clearance. Notably, all compounds were classified as ultra-short half-life drugs ($t_{1/2}$ < 1 h), indicating rapid systemic elimination that could challenge maintaining therapeutic exposure in vivo.

The toxicity predictions indicated that all compounds displayed moderate to high probabilities of toxicity, including AMES (mutagenic) toxicity, hepatotoxicity, and nephrotoxicity. AOH1996 showed even higher predicted AMES and hepatotoxicity probabilities than its derivatives, suggesting that the structural modifications in **2b**, **3b**, **3c**, and **3d** may have partially mitigated intrinsic toxic liability. All compounds showed high probabilities

of hERG inhibition, indicating a potential cardiotoxic liability. For the FDA maximum recommended daily dose (FDAMDD), compound **1f** showed the highest probability (0.735) of being FDAMDD-positive, suggesting a potentially higher tolerated dose range. Compound **2b** displayed a moderate probability (0.52), while for other compounds, a narrower therapeutic window and higher toxicity risk at elevated doses were predicted.

Overall, while these ADMET profiles (Tables 6–8) highlighted significant challenges, particularly related to cardiotoxicity, high plasma binding, and rapid clearance, the derivatives possessed features—such as favorable intestinal absorption, moderate metabolic stability (for **2b** and **3b**), and potential for P-gp inhibition—that justify their consideration as lead scaffolds for further optimization. Future studies could focus on structural modifications or formulation strategies, including targeted or nanoformulated delivery, to mitigate these limitations while maintaining antiproliferative activity.

Table 6. ADMET predicted medicinal chemistry and absorption data.

	Medicinal Chemistry					Absorption		
	Lipinski (MW ≤ 500; logP ≤ 5; etc.)	Pfizer rule (logP > 3; TPSA < 75)	GSK rule (MW ≤ 400; logP ≤ 4)	Golden triangle (200 ≤ MW ≤ 500; −2 ≤ logD ≤ 5)		Human intestinal absorption	Caco2 permeability (Optimal: higher than −5.15 Log unit)	P-gp substrate/inhibitor
1f	yes	yes	no	yes	**1f**	≥30%	yes	no
2b	yes	yes	yes	yes	**2b**	≥30%	yes	inhibitor
3c	yes	yes	no	yes	**3c**	≥30%	yes	no
3b	yes	yes	yes	yes	**3b**	≥30%	yes	inhibitor
3d	yes	yes	no	yes	**3d**	≥30%	yes	inhibitor
AOH1996	yes	yes	no	yes	AOH1996	≥30%	yes	no

Table 7. ADMET predicted distribution and metabolism probabilities.

	Distribution				Metabolism				
	Volume distribution (optimal: 0.04–20 L/kg)	BBB permeability Log BB (probability of being BBB+)	Plasma protein binding (Optimal: <90%)		Substrate CYP 2D6 (probability)	Substrate CYP 3A4 (probability)	Inhibitor CYP 2D6 (probability)	Inhibitor CYP 3A4 (probability)	Human liver microsomal instability (probability)
1f	0.254	0.595	98.469	**1f**	0.017	0.04	0.003	0.156	0.204
2b	0.057	0.003	98.442	**2b**	0.992	0.164	0.992	1	0.99
3c	−0.049	0.728	98.449	**3c**	0.002	0.001	0.35	1	0.381
3b	0.007	0.568	97.939	**3b**	0	0.005	0.217	1	0.403
3d	−0.014	0.435	98.396	**3d**	0.814	0.025	0.814	0.998	0.988
AOH1996	0.046	0.344	98.687	AOH1996	0.193	0.002	0.867	1	0.793

Table 8. ADMET predicted excretion and toxicity probabilities.

	Excretion			Toxicity				
	CL *	t 1/2 **		AMES toxicity (probability)	Hepatoxicity (probability)	Nephrotoxicity (probability)	hERG+ (probability)	FDA maximum recommended dose (probability)
1f	low	ultra short	**1f**	0.772	0.736	0.829	0.934	0.735
2b	moderate	ultra short	**2b**	0.662	0.619	0.729	0.936	0.52
3c	moderate	ultra short	**3c**	0.643	0.673	0.395	0.818	0.229
3b	moderate	ultra short	**3b**	0.794	0.763	0.627	0.835	0.213
3d	moderate	ultra short	**3d**	0.549	0.646	0.585	0.906	0.296
AOH1996	moderate	ultra short	AOH1996	0.806	0.712	0.45	0.878	0.303

* (>15 mL/min/kg: high clearance; 5–15 mL/min/kg: moderate clearance; <5 mL/min/kg: low clearance). ** (ultra-short half-life drugs: 1/2 < 1 h; short half-life drugs: T1/2 between 1–4 h; intermediate short half-life drugs: T1/2 between 4–8 h; long half-life drugs: T1/2 > 8 h).

3.4. Chemical Synthesis

^{1}H (400 MHz), ^{13}C (101 MHz), HSQC, and HMBC NMR spectra were recorded using a Bruker 400 spectrometer (Bruker, Leipzig, Germany). Residual values of deuterated solvents or TMS were used as internal standards. Chemical shift values are given on the δ (ppm) scale. The following symbols are used to describe the NMR spectra: s—singlet, d—doublet, t—triplet, dt—doublet of triplets, dd—doublet of doublets, td—triplet of doublets, ddd—doublet of doublet of doublets and m—multiplet. Melting points of compounds were determined in open capillaries using a Stuart SMP 10 (Cole-Parmer, Stone, Staffordshire, UK) instrument and are uncorrected. The progress of the reactions was monitored using a Shimadzu GCMS-QP2050 (Shimadzu, Kyoto, Japan) and thin-layer chromatography using TLC silica gel 60 F254 plates (Merck, Darmstadt, Germany). HRMS spectra were obtained on a mass spectrometer (Dual-ESI Q-TOF 6520 (Agilent Technologies, Santa Clara, CA, USA). Eluents included mixtures of hexane, ethyl acetate, methanol, and dichloromethane at various ratios. Vanillin, ninhydrin, UV light, and potassium permanganate were used to develop the TLC plates.

2-Azido-*N*-(2-(3-methoxyphenoxy)phenyl)acetamide, 2-chloro-*N*-(2-(3-methoxyphenoxy) phenyl)acetamide, 2-amino-*N*-(2-(3-methoxyphenoxy)phenyl)acetamide, and AOH1996 were prepared in our laboratory by our developed and yet unpublished procedures.

General procedure for synthesis of *N*-(2-(3-methoxyphenoxy)phenyl)-2-(4-substituted-1*H*-1,2,3-triazol-1-yl)acetamides (**1a**–**g**):

Into a 100 mL round-bottomed flask with a reflux condenser, magnetic stirrer, and thermocouple was added 1 eq (2 g, 6.7 mmol) of starting 2-azido-*N*-(2-(3-methoxyphenoxy) phenyl)acetamide and 1.6 eq (10.72 mmol) of 4-substituted phenylacetylene, unsubstituted phenylacetylene, 4-ethynyl-1,1′-biphenyl, or 5-chloropent-1-yne, followed by the addition of 30 mL of dimethylformamide and 0.15 eq (1 mmol) of copper(I) iodide. The reaction mixture was heated in an oil bath at 80 °C for 24 h. The reaction was performed under an inert atmosphere of argon. After 24 h, the reaction mixture was poured into brine and extracted with MTBE. The separated organic layer was dried over anhydrous sodium sulfate, filtered, and then evaporated under reduced pressure. The resulting solid was crystallized from isopropanol or ethanol depending on the substrate.

- 2-(4-(3-Chloropropyl)-1*H*-1,2,3-triazol-1-yl)-*N*-(2-(3-methoxyphenoxy)phenyl)acetamide (**1a**)

  White crystals, m.p. 112–115 °C (*i*PrOH), Yield 2 g (74%).

  ^{1}H NMR (400 MHz, $CDCl_3$) δ (ppm): 8.32 (dd, *J* = 8.0, 1.7 Hz, 1H, H_{Ar}), 8.12 (s, 1H, NH), 7.45 (s, 1H, H_{HAr}), 7.25–7.15 (m, 1H, H_{Ar}), 7.15–7.02 (m, 2H, H_{Ar}), 6.89 (dd, *J* = 8.0, 1.5 Hz, 1H, H_{Ar}), 6.71–6.64 (m, 1H, H_{Ar}), 6.52–6.45 (m, 2H, H_{Ar}), 5.16 (s, 2H, NCH_2), 3.79 (s, 3H, OCH_3), 3.52 (t, *J* = 6.3 Hz, 2H, CH_2Cl), 2.85 (t, *J* = 7.4 Hz, 2H, CCH_2), 2.15–2.04 (m, 2H, $CH_2\underline{CH_2}CH_2$).

  ^{13}C NMR (101 MHz, $CDCl_3$) δ (ppm): 163.21 (CO), 161.03 (C_{Ar}), 157.23 (C_{Ar}), 147.32 (C_{Ar}), 145.55 (C_{Ar}), 130.35 (C_{Ar}), 128.59 (C_{Ar}), 125.20 (C_{Ar}), 124.24 (C_{Ar}), 122.61 (C_{Ar}), 121.06 (C_{Ar}), 118.34 (C_{Ar}), 110.21 (C_{Ar}), 109.55 (C_{Ar}), 104.42 (C_{Ar}), 55.45 (OCH_3), 53.60 (NCH_2), 44.08 (CH_2Cl), 31.63 (CCH_2), 22.55 ($CH_2\underline{C}H_2CH_2$).

  HRMS (ESI) *m*/*z*: $[M+Na]^+$ calcd for $C_{20}H_{21}ClN_4NaO_3$, 423.1200; found, 423.1198 (error = −0.45 ppm).

- *N*-(2-(3-Methoxyphenoxy)phenyl)-2-(4-phenyl-1*H*-1,2,3-triazol-1-yl)acetamide (**1b**)

  White crystals, m.p. 83–86 °C (*i*PrOH), Yield 1 g (50%).

  ^{1}H NMR (400 MHz, $CDCl_3$) δ (ppm): 8.32 (dd, *J* = 8.1, 1.7 Hz, 1H, H_{Ar}), 8.22 (s, 1H, NH), 7.87 (s, 1H, H_{HAr}), 7.81–7.71 (m, 2H, H_{Ar}), 7.48–7.38 (m, 2H, H_{Ar}), 7.39–7.30 (m, 1H,

H_{Ar}), 7.18–7.01 (m, 3H, H_{Ar}), 6.90 (dd, *J* = 8.1, 1.5 Hz, 1H, H_{Ar}), 6.64–6.54 (m, 1H, H_{Ar}), 6.48–6.38 (m, 2H, H_{Ar}), 5.22 (s, 2H, NCH_2), 3.68 (s, 3H, OCH_3).

^{13}C NMR (101 MHz, $CDCl_3$) δ (ppm): 163.15 (CO), 160.93 (C_{Ar}), 157.27 (C_{Ar}), 148.57 (C_{Ar}), 145.49 (C_{Ar}), 130.27 (C_{Ar}), 129.99 (C_{Ar}), 128.83 (C_{Ar}), 128.71 (C_{Ar}), 128.43 (C_{Ar}), 125.86 (C_{Ar}), 125.29 (C_{Ar}), 124.34 (C_{Ar}), 121.23 (C_{Ar}), 121.01 (C_{Ar}), 118.66 (C_{Ar}), 109.90 (C_{Ar}), 109.48 (C_{Ar}), 103.99 (C_{Ar}), 55.30 (OCH_3), 53.72 (NCH_2).

HRMS (ESI) *m*/*z*: $[M+H]^+$ calcd for $C_{23}H_{21}N_4O_3$, 401.1614; found, 401.1616 (error = 0.58 ppm).

- 2-(4-(4-Fluorophenyl)-1*H*-1,2,3-triazol-1-yl)-*N*-(2-(3-methoxyphenoxy)phenyl)acetamide (**1c**)

White crystals, m.p. 104–108 °C (*i*PrOH), Yield 1.5 g (54%).

^1H NMR (400 MHz, $CDCl_3$) δ (ppm): 8.33 (d, *J* = 8.0 Hz, 1H, H_{Ar}), 8.12 (s, 1H, NH), 7.83 (s, 1H, H_{HAr}), 7.79–7.68 (m, 2H, H_{Ar}), 7.55–7.44 (m, 3H, H_{Ar}), 7.18–7.12 (m, 2H, H_{Ar}), 6.91 (d, *J* = 8.0 Hz, 1H, H_{Ar}), 6.65–6.52 (m, 1H, H_{Ar}), 6.48–6.36 (m, 2H, H_{Ar}), 5.23 (s, 2H, NCH_2), 3.71 (s, 3H, OCH_3).

^{13}C NMR (101 MHz, $CDCl_3$) δ (ppm): 162.98 (CO), 160.97 (C_{Ar}), 157.26 (C_{Ar}), 147.48 (C_{Ar}), 145.42 (C_{Ar}), 134.54 (d, *J* = 8.6 Hz, C_{Ar}), 130.29 (C_{Ar}), 128.66 (C_{Ar}), 127.63 (d, *J* = 7.9 Hz, C_{Ar}), 126.23 (C_{Ar}), 125.33 (C_{Ar}), 124.39 (C_{Ar}), 121.13 (C_{Ar}), 120.69 (C_{Ar}), 118.64 (C_{Ar}), 117.82 (C_{Ar}), 109.89 (C_{Ar}), 109.44 (C_{Ar}), 104.08 (C_{Ar}), 55.33 (OCH_3), 53.78 (NCH_2).

HRMS (ESI) *m*/*z*: $[M+H]^+$ calcd for $C_{23}H_{20}FN_4O_3$, 419.1519; found, 419.1510 (error = −2.25 ppm).

- *N*-(2-(3-Methoxyphenoxy)phenyl)-2-(4-(4-methoxyphenyl)-1*H*-1,2,3-triazol-1-yl) acetamide (**1d**)

White crystals, m.p. 138–141 °C (*i*PrOH), Yield 2 g (69%).

^1H NMR (400 MHz, $CDCl_3$) δ (ppm): 8.32 (dd, *J* = 8.1, 1.7 Hz, 1H, H_{Ar}), 8.20 (s, 1H, NH), 7.77 (s, 1H, H_{Ar}), 7.72–7.65 (m, 2H, H_{Ar}), 7.51–7.40 (m, 1H, H_{Ar}), 7.18–7.03 (m, 3H, H_{Ar}), 6.90 (dd, *J* = 8.0, 1.5 Hz, 1H, H_{Ar}), 6.88–6.78 (m, 1H, H_{Ar}), 6.65–6.54 (m, 1H, H_{Ar}), 6.48–6.38 (m, 2H, H_{Ar}), 5.20 (s, 2H, NCH_2), 3.85 (s, 3H, OCH_3), 3.69 (s, 3H, OCH_3).

^{13}C NMR (101 MHz, $CDCl_3$) δ (ppm): 163.22 (CO), 160.94 (C_{Ar}), 159.79 (C_{Ar}), 157.27 (C_{Ar}), 148.48 (C_{Ar}), 145.48 (C_{Ar}), 134.04 (C_{Ar}), 130.26 (C_{Ar}), 128.72 (C_{Ar}), 127.19 (C_{Ar}), 125.26 (C_{Ar}), 124.34 (C_{Ar}), 122.69 (C_{Ar}), 121.22 (C_{Ar}), 120.16 (C_{Ar}), 118.65 (C_{Ar}), 114.22 (C_{Ar}), 109.48 (C_{Ar}), 103.98 (C_{Ar}), 55.33 (OCH_3), 55.31 (OCH_3), 53.72 (NCH_2).

HRMS (ESI) *m*/*z*: $[M+Na]^+$ calcd for $C_{24}H_{22}N_4NaO_4$, 453.1539; found, 453.1554 (error = 3.37 ppm).

- 2-(4-(4-Ethylphenyl)-1*H*-1,2,3-triazol-1-yl)-*N*-(2-(3-methoxyphenoxy)phenyl)acetamide (**1e**)

White crystals, m.p. 121–124 °C (*i*PrOH), Yield 2.1 g (56%).

^1H NMR (400 MHz, DMSO-d_6) δ (ppm): 8.49 (s, 1H, H_{HAr}), 8.10–8.00 (m, 1H, H_{Ar}), 7.77 (d, *J* = 7.9 Hz, 2H, H_{Ar}), 7.35–7.25 (m, 3H, H_{Ar}), 7.17–7.09 (m, 2H, H_{Ar}), 6.97–6.89 (m, 1H, H_{Ar}), 6.76 (dd, *J* = 8.3, 2.4 Hz, 1H, H_{Ar}), 6.67–6.53 (m, 2H, H_{Ar}), 5.44 (s, 2H, NCH_2), 3.74 (s, 3H, OCH_3), 2.63 (q, 2H, CH_2), 1.20 (t, *J* = 7.6 Hz, 3H, CH_3).

^{13}C NMR (101 MHz, DMSO-d_6) δ (ppm): 165.21 (CO), 161.11 (C_{Ar}), 158.12 (C_{Ar}), 147.71 (C_{Ar}), 147.63 (C_{Ar}), 146.75 (C_{Ar}), 143.95 (C_{Ar}), 130.96 (C_{Ar}), 129.40 (C_{Ar}), 128.77 (C_{Ar}), 128.66 (C_{Ar}), 125.64 (C_{Ar}), 124.20 (C_{Ar}), 123.61 (C_{Ar}), 123.11 (C_{Ar}), 119.17 (C_{Ar}), 111.06 (C_{Ar}), 109.78 (C_{Ar}), 105.31 (C_{Ar}), 55.77 (OCH_3), 52.66 (NCH_2), 28.41 (CH_2), 15.98 (CH_3).

HRMS (ESI) *m*/*z*: $[M+H]^+$ calcd for $C_{25}H_{25}N_4O_3$, 429.1927; found, 429.1915 (error = −2.72 ppm).

- 2-(4-([1,1′-Biphenyl]-4-yl)-1H-1,2,3-triazol-1-yl)-*N*-(2-(3-methoxyphenoxy)phenyl) acetamide (**1f**)

White crystals, m.p. 156–158 °C (*i*PrOH), Yield 2.0 g (63%).

^{1}H NMR (400 MHz, $CDCl_3$) δ (ppm): 8.33 (dd, *J* = 8.1, 1.7 Hz, 1H, H_{Ar}), 8.19 (s, 1H, NH), 7.90 (s, 1H, H_{HAr}), 7.88–7.80 (m, 2H, H_{Ar}), 7.69–7.61 (m, 4H, H_{Ar}), 7.51–7.41 (m, 2H, H_{Ar}), 7.41–7.33 (m, 1H, H_{Ar}), 7.18–7.03 (m, 3H, H_{Ar}), 6.91 (dd, *J* = 8.0, 1.5 Hz, 1H, H_{Ar}), 6.63–6.55 (m, 1H, H_{Ar}), 6.48–6.40 (m, 2H, H_{Ar}), 5.24 (s, 2H, NCH_2), 3.67 (s, 3H, OCH_3).

^{13}C NMR (101 MHz, $CDCl_3$) δ (ppm): 163.11 (CO), 160.96 (C_{Ar}), 157.27 (C_{Ar}), 148.31 (C_{Ar}), 145.47 (C_{Ar}), 141.16 (C_{Ar}), 140.48 (C_{Ar}), 130.28 (C_{Ar}), 128.93 (C_{Ar}), 128.87 (C_{Ar}), 128.70 (C_{Ar}), 127.53 (C_{Ar}), 127.49 (C_{Ar}), 126.98 (C_{Ar}), 126.25 (C_{Ar}), 125.30 (C_{Ar}), 124.36 (C_{Ar}), 121.19 (C_{Ar}), 120.97 (C_{Ar}), 118.65 (C_{Ar}), 109.88 (C_{Ar}), 109.52 (C_{Ar}), 104.01 (C_{Ar}), 55.30 (OCH_3), 53.77 (NCH_2).

HRMS (ESI) *m*/*z*: $[M+Na]^+$ calcd for $C_{29}H_{24}N_4NaO_3$, 499.1746; found, 499.1753 (error = 1.38 ppm).

- *N*-(2-(3-Methoxyphenoxy)phenyl)-2-(4-(4-pentylphenyl)-1*H*-1,2,3-triazol-1-yl)acetamide (**1g**)

White crystals, m.p. 77–80 °C (EtOH), Yield 1.8 g (57%).

^{1}H NMR (400 MHz, DMSO-d_6) δ (ppm): 8.48 (s, 1H, H_{HAr}), 8.03 (q, *J* = 5.0 Hz, 1H, H_{Ar}), 7.75 (d, *J* = 7.9 Hz, 2H, H_{Ar}), 7.30 (t, *J* = 8.2 Hz, 1H, H_{Ar}), 7.27 (s, 1H, H_{Ar}), 7.25 (s, 1H, H_{Ar}), 7.11 (dt, *J* = 9.3, 3.6 Hz, 2H, H_{Ar}), 6.91 (dd, *J* = 6.2, 3.4 Hz, 1H, H_{Ar}), 6.74 (dd, *J* = 8.3, 2.4 Hz, 1H, H_{Ar}), 6.62 (d, *J* = 2.5 Hz, 1H, H_{Ar}), 6.57 (dd, *J* = 8.1, 2.3 Hz, 1H, H_{Ar}), 5.42 (d, *J* = 2.1 Hz, 2H, NCH_2), 3.73 (s, 3H, OCH_3), 2.58 (t, *J* = 7.7 Hz, 2H, CH_2), 1.57 (h, *J* = 6.9, 6.3 Hz, 2H, CH_2), 1.29 (qt, *J* = 8.0, 3.5 Hz, 4H, CH_2CH_2), 0.89–0.80 (m, 3H, CH_3).

^{13}C NMR (101 MHz, DMSO-d_6) δ (ppm): 165.20 (CO), 161.10 (C_{Ar}), 158.11 (C_{Ar}), 147.62 (C_{Ar}), 146.75 (C_{Ar}), 142.56 (C_{Ar}), 132.81 (C_{Ar}), 130.95 (C_{Ar}), 129.29 (C_{Ar}), 128.65 (C_{Ar}), 125.80 (C_{Ar}), 125.58 (C_{Ar}), 124.19 (C_{Ar}), 123.59 (C_{Ar}), 123.10 (C_{Ar}), 119.17 (C_{Ar}), 111.06 (C_{Ar}), 109.78 (C_{Ar}), 105.31 (C_{Ar}), 55.77 (OCH_3), 52.66 (NCH_2), 35.33 (CH_2), 31.36 (CH_2), 31.03 (CH_2), 22.44 (CH_2), 14.41 (CH_3).

HRMS (ESI) *m*/*z*: $[M+H]^+$ calcd for $C_{28}H_{31}N_4O_3$, 471.2396; found, 471.2399 (error = −0.60 ppm).

General procedure for substitution of 2-chloro-*N*-(2-(3-methoxyphenoxy)phenyl)acetamide with various amines (**2a**–**g**):

Into a 100 mL round-bottomed flask with a reflux condenser and magnetic stirrer was added 1 eq (6.87 mmol) of starting 2-chloro-*N*-(2-(3-methoxyphenoxy)phenyl)acetamide and 2.1 eq (4.4 mmol) of a nitrogen atom-containing nucleophile (Table 3), followed by the addition of 30 mL of acetonitrile. The reaction mixture was refluxed for 3 h. After the reaction was finished, the acetonitrile was evaporated under reduced pressure. The resulting solid was extracted with methylene chloride, washed with brine, dried over sodium sulfate, and then evaporated once more under reduced pressure to give a solid, which was crystallized from isopropanol or cyclohexane depending on the substrate.

- 2-(Dimethylamino)-*N*-(2-(3-methoxyphenoxy)phenyl)acetamide (**2a**)

White crystals, m.p. 54–56 °C (cyclohexane), Yield 1.7 g (83%).

^{1}H NMR (400 MHz, $CDCl_3$) δ (ppm): 9.64 (s, 1H, NH), 8.46 (m, 1H, H_{Ar}), 7.26–7.13 (m, 2H, H_{Ar}), 7.06 (m, 1H, H_{Ar}), 6.99 (m, 1H, H_{Ar}), 6.64 (m, 1H, H_{Ar}), 6.58–6.50 (m, 2H, H_{Ar}), 3.77 (s, 3H, OCH_3), 3.01 (s, 2H, NCH_2), 2.19 (s, 6H, CH_3).

^{13}C NMR (101 MHz, $CDCl_3$) δ (ppm): 169.00 (CO), 161.03 (C_{Ar}), 158.41 (C_{Ar}), 144.80 (C_{Ar}), 130.24 (C_{Ar}), 130.13 (C_{Ar}), 124.84 (C_{Ar}), 124.10 (C_{Ar}), 120.97 (C_{Ar}), 119.65 (C_{Ar}), 109.52 (C_{Ar}), 108.73 (C_{Ar}), 103.64 (C_{Ar}), 63.72 (NCH_2), 55.39 (OCH_3), 45.72 (CH_3).

HRMS (ESI) *m*/*z*: [M+H]$^+$ calcd for $C_{17}H_{21}N_2O_3$, 301.1552; found, 301.1557 (error = 1.60 ppm).

- 2-(Aziridin-1-yl)-*N*-(2-(3-methoxyphenoxy)phenyl)acetamide (**2b**)

White crystals, m.p. 75–78 °C (cyclohexane), Yield 1.5 g (63%).

^{1}H NMR (400 MHz, $CDCl_3$) δ (ppm): 9.47 (s, 1H, NH), 8.49 (dd, *J* = 8.1, 1.6 Hz, 1H, H_{Ar}), 7.26–7.12 (m, 2H, H_{Ar}), 7.06 (td, *J* = 7.8, 1.6 Hz, 1H, H_{Ar}), 6.96 (dd, *J* = 8.1, 1.5 Hz, 1H, H_{Ar}), 6.69–6.62 (m, 1H, H_{Ar}), 6.59–6.52 (m, 2H, H_{Ar}), 3.77 (s, 3H, OCH_3), 3.02 (s, 2H, NCH_2CO), 1.74–1.68 (m, 2H, CH_2), 1.28–1.20 (m, 2H, CH_2).

^{13}C NMR (101 MHz, $CDCl_3$) δ (ppm): 168.70 (CO), 161.02 (C_{Ar}), 158.11 (C_{Ar}), 145.16 (C_{Ar}), 130.26 (C_{Ar}), 129.93 (C_{Ar}), 124.60 (C_{Ar}), 124.24 (C_{Ar}), 120.91 (C_{Ar}), 119.06 (C_{Ar}), 109.94 (C_{Ar}), 108.99 (C_{Ar}), 103.99 (C_{Ar}), 64.24 ($N\underline{C}H_2CO$), 55.40 (OCH_3), 27.74 (CH_2).

HRMS (ESI) *m*/*z*: [M+Na]$^+$ calcd for $C_{17}H_{18}N_2NaO_3$, 321.1215; found, 321.1214 (error = −0.35 ppm).

- 2-(Azetidin-1-yl)-*N*-(2-(3-methoxyphenoxy)phenyl)acetamide (**2c**)

White crystals, m.p. 91–94 °C (*i*PrOH), Yield 1.7 g (73%).

^{1}H NMR (400 MHz, $CDCl_3$) δ (ppm): 9.56 (s, 1H, NH), 8.47 (dd, *J* = 8.2, 1.6 Hz, 1H, H_{Ar}), 7.26–7.12 (m, 2H, H_{Ar}), 7.05 (td, *J* = 7.6, 7.2, 1.6 Hz, 1H, H_{Ar}), 7.00 (dd, *J* = 8.1, 1.7 Hz, 1H, H_{Ar}), 6.65 (ddd, *J* = 8.3, 2.4, 0.9 Hz, 1H, H_{Ar}), 6.61–6.52 (m, 2H, H_{Ar}), 3.78 (s, 3H, OCH_3), 3.20–3.12 (m, 6H, $C\underline{H}_2CH_2C\underline{H}_2$ and $NC\underline{H}_2CO$), 1.96 (p, *J* = 7.0 Hz, 2H, $CH_2C\underline{H}_2CH_2$).

^{13}C NMR (101 MHz, $CDCl_3$) δ (ppm): 168.72 (CO), 161.09 (C_{Ar}), 158.56 (C_{Ar}), 144.46 (C_{Ar}), 130.33 (C_{Ar}), 130.28 (C_{Ar}), 124.99 (C_{Ar}), 124.04 (C_{Ar}), 120.81 (C_{Ar}), 119.89 (C_{Ar}), 109.21 (C_{Ar}), 108.67 (C_{Ar}), 103.39 (C_{Ar}), 63.28 ($N\underline{C}H_2CO$), 55.76 ($\underline{C}H_2CH_2\underline{C}H_2$), 55.40 ($OCH_3$), 17.49 ($CH_2\underline{C}H_2CH_2$).

HRMS (ESI) *m*/*z*: [M+H]$^+$ calcd for $C_{18}H_{21}N_2O_3$, 313.1552; found, 313.1564 (error = 3.77 ppm).

- 2-(Benzyl(methyl)amino)-*N*-(2-(3-methoxyphenoxy)phenyl)acetamide (**2d**)

Yellow oil, Yield 2 g (78%).

^{1}H NMR (400 MHz, $CDCl_3$) δ (ppm): 9.86 (s, 1H, NH), 8.50 (dd, *J* = 8.1, 1.6 Hz, 1H, H_{Ar}), 7.28–7.10 (m, 7H, H_{Ar}), 7.04 (td, *J* = 7.8, 1.6 Hz, 1H, H_{Ar}), 7.01–6.93 (m, 1H, H_{Ar}), 6.68 (ddd, *J* = 8.3, 2.3, 1.0 Hz, 1H, H_{Ar}), 6.63–6.56 (m, 2H, H_{Ar}), 3.75 (s, 3H, OCH_3), 3.57 (s, 2H, $PhC\underline{H}_2$), 3.13 (s, 2H, $NC\underline{H}_2CO$), 2.18 (s, 3H, NCH_3).

^{13}C NMR (101 MHz, $CDCl_3$) δ (ppm): 169.11 (CO), 161.09 (C_{Ar}), 158.16 (C_{Ar}), 144.94 (C_{Ar}), 137.86 (C_{Ar}), 130.35 (C_{Ar}), 130.05 (C_{Ar}), 128.76 (C_{Ar}), 128.44 (C_{Ar}), 127.41 (C_{Ar}), 124.59 (C_{Ar}), 123.97 (C_{Ar}), 120.49 (C_{Ar}), 118.93 (C_{Ar}), 110.00 (C_{Ar}), 109.10 (C_{Ar}), 104.02 (C_{Ar}), 62.30 ($N\underline{C}H_2CO$), 61.33 ($Ph\underline{C}H_2$), 55.39 (OCH_3), 42.99 (NCH_3).

HRMS (ESI) *m*/*z*: [M+H]$^+$ calcd for $C_{23}H_{25}N_2O_3$, 377.1865; found, 377.1852 (error = −3.49 ppm).

- *N*-(2-(3-Methoxyphenoxy)phenyl)-2-(pyrrolidin-1-yl)acetamide (**2e**)

White crystals, m.p. 88–91 °C (*i*PrOH), Yield 1.5 g (67%).

^{1}H NMR (400 MHz, $CDCl_3$) δ (ppm): 9.71 (s, 1H, NH), 8.49 (dd, *J* = 8.2, 1.6 Hz, 1H, H_{Ar}), 7.24–7.15 (m, 2H, H_{Ar}), 7.06 (td, *J* = 7.8, 1.6 Hz, 1H, H_{Ar}), 7.01 (dd, *J* = 8.1, 1.6 Hz, 1H, H_{Ar}), 6.62 (ddd, *J* = 8.3, 2.4, 0.9 Hz, 1H, H_{Ar}), 6.54–6.45 (m, 2H, H_{Ar}), 3.77 (s, 3H, OCH_3), 3.22 (s, 2H, $NC\underline{H}_2CO$), 2.54–2.45 (m, 4H, $C\underline{H}_2CH_2CH_2C\underline{H}_2$), 1.64 (dd, *J* = 10.0, 3.3 Hz, 4H, $CH_2C\underline{H}_2C\underline{H}_2CH_2$).

^{13}C NMR (101 MHz, $CDCl_3$) δ (ppm): 169.38 (CO), 161.00 (C_{Ar}), 158.63 (C_{Ar}), 144.17 (C_{Ar}), 130.59 (C_{Ar}), 130.25 (C_{Ar}), 125.17 (C_{Ar}), 124.06 (C_{Ar}), 120.79 (C_{Ar}), 120.13 (C_{Ar}), 108.76 (C_{Ar}), 108.43 (C_{Ar}), 102.97 (C_{Ar}), 59.53 ($N\underline{C}H_2CO$), 55.37 (OCH_3), 54.30 ($\underline{C}H_2CH_2CH_2\underline{C}H_2$), 23.97 ($CH_2\underline{C}H_2\underline{C}H_2CH_2$).

HRMS (ESI) *m*/*z*: $[M+H]^+$ calcd for $C_{19}H_{23}N_2O_3$, 327.1709; found, 327.1715 (error = 1.93 ppm).

- *N*-(2-(3-Methoxyphenoxy)phenyl)-2-(piperidin-1-yl)acetamide (**2f**)

White crystals, m.p. 89–92 °C (*i*PrOH), Yield 1.5 g (80%).

^{1}H NMR (400 MHz, $CDCl_3$) δ (ppm): 9.90 (s, 1H, NH), 8.50 (dd, *J* = 8.2, 1.6 Hz, 1H, H_{Ar}), 7.28–7.14 (m, 2H, H_{Ar}), 7.04 (td, *J* = 7.8, 1.6 Hz, 1H, H_{Ar}), 6.98 (dd, *J* = 8.2, 1.6 Hz, 1H, H_{Ar}), 6.64 (ddd, *J* = 8.3, 2.3, 1.0 Hz, 1H, H_{Ar}), 6.58–6.50 (m, 2H, H_{Ar}), 3.77 (s, 3H, OCH_3), 3.03 (s, 2H, $NC\underline{H_2}CO$), 2.42 (t, *J* = 5.0 Hz, 4H, $C\underline{H_2}CH_2CH_2CH_2C\underline{H_2}$), 1.45–1.30 (m, 6H, $CH_2C\underline{H_2}C\underline{H_2}C\underline{H_2}CH_2$).

^{13}C NMR (101 MHz, $CDCl_3$) δ (ppm): 169.29 (CO), 161.02 (C_{Ar}), 158.40 (C_{Ar}), 144.58 (C_{Ar}), 130.41 (C_{Ar}), 130.25 (C_{Ar}), 124.86 (C_{Ar}), 123.99 (C_{Ar}), 120.66 (C_{Ar}), 119.50 (C_{Ar}), 109.36 (C_{Ar}), 108.67 (C_{Ar}), 103.50 (C_{Ar}), 62.92 ($N\underline{C}H_2CO$), 55.37 (OCH_3), 54.84 ($\underline{C}H_2CH_2CH_2CH_2\underline{C}H_2$), 26.01 ($CH_2\underline{C}H_2CH_2\underline{C}H_2CH_2$), 23.57 ($CH_2CH_2\underline{C}H_2CH_2CH_2$).

HRMS (ESI) *m*/*z*: $[M+H]^+$ calcd for $C_{20}H_{25}N_2O_3$, 341.1865; found, 341.1852 (error = −3.86 ppm).

- *N*-(2-(3-Methoxyphenoxy)phenyl)-2-morpholinoacetamide (**2g**)

White crystals, m.p. 114–117 °C (*i*PrOH), Yield 1.8 g (78%).

^{1}H NMR (400 MHz, $CDCl_3$) δ (ppm): 9.72 (s, 1H, NH), 8.48 (dd, *J* = 8.2, 1.6 Hz, 1H, H_{Ar}), 7.26–7.14 (m, 2H, H_{Ar}), 7.07 (td, *J* = 7.8, 1.6 Hz, 1H, H_{Ar}), 6.99 (dd, *J* = 8.1, 1.5 Hz, 1H, H_{Ar}), 6.64 (ddd, *J* = 8.3, 2.3, 1.1 Hz, 1H, H_{Ar}), 6.57–6.50 (m, 2H, H_{Ar}), 3.77 (s, 3H, OCH_3), 3.51 (t, *J* = 4.6 Hz, 4H, $C\underline{H_2}OC\underline{H_2}$), 3.10 (s, 2H, $NC\underline{H_2}CO$), 2.48 (t, *J* = 4.6 Hz, 4H, $C\underline{H_2}NC\underline{H_2}$).

^{13}C NMR (101 MHz, $CDCl_3$) δ (ppm): 168.13 (CO), 161.10 (C_{Ar}), 158.39 (C_{Ar}), 144.43 (C_{Ar}), 130.40 (C_{Ar}), 130.26 (C_{Ar}), 125.07 (C_{Ar}), 124.33 (C_{Ar}), 120.72 (C_{Ar}), 119.75 (C_{Ar}), 109.16 (C_{Ar}), 108.53 (C_{Ar}), 103.35 (C_{Ar}), 66.83 ($\underline{C}H_2O\underline{C}H_2$), 62.47 ($N\underline{C}H_2CO$), 55.41 ($OCH_3$), 53.65 ($\underline{C}H_2N\underline{C}H_2$).

HRMS (ESI) *m*/*z*: $[M+H]^+$ calcd for $C_{19}H_{23}N_2O_4$, 343.1658; found, 343.1649 (error = −2.57 ppm).

General procedure for amide formation from 2-amino-*N*-(2-(3-methoxyphenoxy)phenyl) acetamide and various substituted benzoyl chlorides (**3a**–**f**):

Into a 100 mL round-bottomed flask with a reflux condenser, magnetic stirrer, thermocouple, and dropping funnel was added 1 eq (7.4 mmol) of starting 2-amino-*N*-(2-(3-methoxyphenoxy)phenyl)acetamide and 30 mL of methylene chloride. Then, the reaction mixture was cooled to −50 °C, and 1.05 eq (7.7 mmol) of the corresponding benzoyl chloride was added. Subsequently, 1.07 eq (7.9 mmol) of triethylamine was slowly added to the reaction mixture, maintaining the same temperature. After triethylamine addition, the reaction mixture was stirred for another hour and then for 24 h at room temperature. After the reaction ended, the reaction mixture was washed with water, then with saturated potassium carbonate solution and brine until a pH value of 8–9 was reached. The organic layer was dried over sodium sulfate and evaporated under reduced pressure to give a solid, which was crystallized from isopropanol.

- *N*-(2-((2-(3-Methoxyphenoxy)phenyl)amino)-2-oxoethyl)-4-nitrobenzamide (**3a**)

Yellowish crystals, m.p. 134–136 °C (*i*PrOH), Yield 2.5 g (80%).

^{1}H NMR (400 MHz, $CDCl_3$) δ (ppm): 8.56 (s, 1H, $NHCH_2CON\underline{H}$), 8.30 (dd, *J* = 7.9, 1.8 Hz, 1H, H_{Ar}), 8.22–8.14 (m, 2H, H_{Ar}), 7.95–7.87 (m, 2H, H_{Ar}), 7.67 (t, *J* = 5.4 Hz, 1H, $N\underline{H}CH_2CONH$), 7.22–7.13 (m, 1H, H_{Ar}), 7.14–7.01 (m, 2H, H_{Ar}), 6.90 (dd, *J* = 7.9, 1.7 Hz, 1H, H_{Ar}), 6.67–6.59 (m, 1H, H_{Ar}), 6.54–6.47 (m, 2H, H_{Ar}), 4.30 (d, *J* = 5.2 Hz, 2H, $C\underline{H_2}CO$), 3.73 (s, 3H, OCH_3).

^{13}C NMR (101 MHz, $CDCl_3$) δ (ppm): 167.15 ($CH_2\underline{C}O$), 165.86 (CO), 161.04 (C_{Ar}), 157.47 (C_{Ar}), 149.74 (C_{Ar}), 145.75 (C_{Ar}), 138.75 (C_{Ar}), 130.37 (C_{Ar}), 129.05 (C_{Ar}), 128.41 (C_{Ar}), 124.99 (C_{Ar}), 124.17 (C_{Ar}), 123.72 (C_{Ar}), 121.24 (C_{Ar}), 118.45 (C_{Ar}), 110.35 (C_{Ar}), 109.25 (C_{Ar}), 104.75 (C_{Ar}), 55.38 (OCH_3), 44.82 ($\underline{C}H_2CO$).

HRMS (ESI) *m*/*z*: $[M+H]^+$ calcd for $C_{22}H_{20}N_3O_6$, 422.1352; found, 422.1365 (error = 3.05 ppm).

- 2-Fluoro-*N*-(2-((2-(3-methoxyphenoxy)phenyl)amino)-2-oxoethyl)benzamide (**3b**)

White crystals, m.p. 93–95 °C (*i*PrOH), Yield 2.5 g (80%).

^{1}H NMR (400 MHz, $CDCl_3$) δ (ppm): 8.43 (s, 1H, $NHCH_2CON\underline{H}$), 8.41 (dd, *J* = 8.1, 1.6 Hz, 1H, H_{Ar}), 7.99 (td, *J* = 7.9, 1.9 Hz, 1H, H_{Ar}), 7.53–7.46 (m, 2H, H_{Ar} and $N\underline{H}CH_2CONH$), 7.29–7.20 (m, 1H, H_{Ar}), 7.20–7.13 (m, 2H, H_{Ar}), 7.13–7.07 (m, 1H, H_{Ar}), 7.04 (td, *J* = 7.8, 1.6 Hz, 1H, H_{Ar}), 6.92 (dd, *J* = 8.1, 1.5 Hz, 1H, H_{Ar}), 6.64–6.57 (m, 1H, H_{Ar}), 6.52–6.45 (m, 2H, H_{Ar}), 4.30 (dd, *J* = 5.4, 1.3 Hz, 2H, $C\underline{H}_2CO$), 3.73 (s, 3H, OCH_3).

^{13}C NMR (101 MHz, $CDCl_3$) δ (ppm): 166.86 ($CH_2\underline{C}O$), 163.82 (d, *J* = 3.0 Hz, CO), 162.01 (C_{Ar}), 160.95 (C_{Ar}), 159.54 (C_{Ar}), 157.66 (C_{Ar}), 145.20 (C_{Ar}), 133.77 (d, *J* = 9.4 Hz, C_{Ar}), 132.07 (d, *J* = 1.9 Hz, C_{Ar}), 130.24 (C_{Ar}), 129.55 (C_{Ar}), 124.78 (d, *J* = 3.3 Hz, C_{Ar}), 124.52 (C_{Ar}), 124.40 (C_{Ar}), 121.06 (C_{Ar}), 118.63 (C_{Ar}), 116.09 (d, *J* = 24.6 Hz, C_{Ar}), 110.00 (C_{Ar}), 109.29 (C_{Ar}), 104.07 (C_{Ar}), 55.33 (OCH_3), 44.89 ($\underline{C}H_2CO$).

HRMS (ESI) *m*/*z*: $[M+H]^+$ calcd for $C_{22}H_{20}FN_2O_4$, 395.1407; found, 395.1409 (error = 0.48 ppm).

- 2-Chloro-*N*-(2-((2-(3-methoxyphenoxy)phenyl)amino)-2-oxoethyl)benzamide (**3c**)

Yellow oil, Yield 2.5 g (74%).

^{1}H NMR (400 MHz, $CDCl_3$) δ (ppm): 8.47 (s, 1H, $NHCH_2CON\underline{H}$), 8.36 (dd, *J* = 8.1, 1.7 Hz, 1H, H_{Ar}), 7.59–7.52 (m, 1H, H_{Ar}), 7.40–7.31 (m, 2H, H_{Ar}), 7.28–7.23 (m, 1H, H_{Ar}), 7.23–7.15 (m, 2H, H_{Ar} and $N\underline{H}CH_2CONH$), 7.10 (td, *J* = 7.8, 1.5 Hz, 1H, H_{Ar}), 7.03 (td, *J* = 7.8, 1.7 Hz, 1H, H_{Ar}), 6.88 (dd, *J* = 8.1, 1.5 Hz, 1H, H_{Ar}), 6.69–6.61 (m, 1H, H_{Ar}), 6.57–6.50 (m, 2H, H_{Ar}), 4.26 (d, *J* = 5.4 Hz, 2H, $C\underline{H}_2CO$), 3.73 (s, 3H, OCH_3).

^{13}C NMR (101 MHz, $CDCl_3$) δ (ppm): 166.90 (CO), 166.79 (CO), 160.99 (C_{Ar}), 157.45 (C_{Ar}), 145.69 (C_{Ar}), 133.89 (C_{Ar}), 131.65 (C_{Ar}), 130.85 (C_{Ar}), 130.32 (C_{Ar}), 130.32 (C_{Ar}), 130.25 (C_{Ar}), 129.14 (C_{Ar}), 127.03 (C_{Ar}), 124.59 (C_{Ar}), 124.08 (C_{Ar}), 121.18 (C_{Ar}), 118.13 (C_{Ar}), 110.55 (C_{Ar}), 109.56 (C_{Ar}), 104.62 (C_{Ar}), 55.36 (OCH_3), 44.67 ($\underline{C}H_2CO$).

HRMS (ESI) *m*/*z*: $[M+H]^+$ calcd for $C_{22}H_{20}ClN_2O_4$, 411.1112; found, 411.1123 (error = 2.77 ppm).

- *N*-(2-((2-(3-Methoxyphenoxy)phenyl)amino)-2-oxoethyl)-4-phenylbutanamide (**3d**)

White crystals, m.p. 106–109 °C (*i*PrOH), Yield 2.7 g (90%).

^{1}H NMR (400 MHz, $CDCl_3$) δ (ppm): 8.38–8.31 (m, 2H, $NHCH_2CON\underline{H}$ + H_{Ar}), 7.30–7.05 (m, 7H, $N\underline{H}CH_2CONH$ + H_{Ar}), 7.03 (td, *J* = 7.8, 1.7 Hz, 1H, H_{Ar}), 6.89 (dd, *J* = 8.1, 1.5 Hz, 1H, H_{Ar}), 6.69–6.62 (m, 1H, H_{Ar}), 6.57–6.50 (m, 2H, H_{Ar}), 6.31 (t, *J* = 5.3 Hz, 1H, H_{Ar}), 4.03 (d, *J* = 5.4 Hz, 2H, $NC\underline{H}_2CO$), 3.74 (s, 3H, OCH_3), 2.60 (t, *J* = 7.5 Hz, 2H, $C\underline{H}_2CH_2CH_2CO$), 2.18 (dd, *J* = 8.3, 6.8 Hz, 2H, $CH_2CH_2C\underline{H}_2CO$), 1.98–1.86 (m, 2H, $CH_2C\underline{H}_2CH_2$).

^{13}C NMR (101 MHz, $CDCl_3$) δ (ppm): 173.37 ($CH_2CH_2\underline{C}O$), 167.27 (CO), 161.06 (C_{Ar}), 157.56 (C_{Ar}), 145.54 (C_{Ar}), 141.31 (C_{Ar}), 130.36 (C_{Ar}), 129.30 (C_{Ar}), 128.48 (C_{Ar}), 128.39 (C_{Ar}), 125.99 (C_{Ar}), 124.54 (C_{Ar}), 124.19 (C_{Ar}), 121.08 (C_{Ar}), 118.32 (C_{Ar}), 110.44 (C_{Ar}), 109.47 (C_{Ar}), 104.54 (C_{Ar}), 55.38 (OCH_3), 44.26 ($N\underline{C}H_2CO$), 35.39 ($CH_2CH_2\underline{C}H_2CO$), 35.15 ($\underline{C}H_2CH_2CH_2CO$), 26.90 ($CH_2\underline{C}H_2CH_2$).

HRMS (ESI) *m*/*z*: $[M+H]^+$ calcd for $C_{25}H_{27}N_2O_4$, 419.1971; found, 419.1977 (error = 1.47 ppm).

- 2-((4,6-Dichloro-1,3,5-triazin-2-yl)amino)-*N*-(2-(3-methoxyphenoxy)phenyl)acetamide (**3e**)

White crystals, m.p. 160–164 °C (*i*PrOH), Yield 0.67 g (22%).

^{1}H NMR (400 MHz, DMSO-d_6) δ (ppm): 9.56 (s, 1H, NH), 9.24 (t, *J* = 6.2 Hz, 1H, $CH_2N\underline{H}$), 8.00–7.87 (m, 1H, H_{Ar}), 7.19 (t, *J* = 8.3 Hz, 1H, H_{Ar}), 7.11–6.99 (m, 2H, H_{Ar}), 6.88–6.80 (m, 1H, H_{Ar}), 6.68–6.60 (m, 1H, H_{Ar}), 6.53–6.45 (m, 1H, H_{Ar}), 6.47–6.41 (m, 1H, H_{Ar}), 4.09 (d, *J* = 6.1 Hz, 2H, $C\underline{H_2}CO$), 3.66 (s, 3H, OCH_3).

^{13}C NMR (101 MHz, DMSO-d_6) δ (ppm): 169.89 ($N\underline{C}NH$), 169.16 (CCl), 167.10 (CO), 161.05 (C_{Ar}), 158.20 (C_{Ar}), 147.53 (C_{Ar}), 130.83 (C_{Ar}), 129.88 (C_{Ar}), 125.61 (C_{Ar}), 124.32 (C_{Ar}), 123.85 (C_{Ar}), 119.46 (C_{Ar}), 110.72 (C_{Ar}), 109.55 (C_{Ar}), 104.94 (C_{Ar}), 55.74 (OCH_3), 44.59 ($\underline{C}H_2CO$).

HRMS (ESI) *m*/*z*: $[M+H]^+$ calcd for $C_{18}H_{16}Cl_2N_5O_3$, 420.0630; found, 420.0633 (error = 0.66 ppm).

- 2-((6-Chloro-1,2,4,5-tetrazin-3-yl)amino)-*N*-(2-(3-methoxyphenoxy)phenyl)acetamide (**3f**)

Orange crystals, m.p. 166–169 °C (*i*PrOH), Yield 0.62 g (32%).

^{1}H NMR (400 MHz, $CDCl_3$) δ (ppm): 8.38 (d, *J* = 8.1 Hz, 1H, $CH_2N\underline{H}$), 8.11 (s, 1H, $CON\underline{H}$), 7.24–7.11 (m, 2H, H_{Ar}), 7.11–7.03 (m, 1H, H_{Ar}), 6.95–6.88 (m, 1H, H_{Ar}), 6.72–6.63 (m, 2H, H_{Ar}), 6.53–6.46 (m, 2H, H_{Ar}), 4.37 (d, *J* = 5.5 Hz, 2H, $C\underline{H_2}CO$), 3.78 (s, 3H, OCH_3).

^{13}C NMR (101 MHz, $CDCl_3$) δ (ppm): 165.39 (CO), 161.19 (C_{Ar}), 161.09 (C_{Ar}), 157.37 (C_{Ar}), 145.27 (C_{Ar}), 130.48 (C_{Ar}), 128.96 (C_{Ar}), 124.96 (C_{Ar}), 124.49 (C_{Ar}), 121.08 (C_{Ar}), 118.55 (C_{Ar}), 110.06 (C_{Ar}), 109.51 (C_{Ar}), 104.29 (C_{Ar}), 102.09 (C_{Ar}), 55.45 (OCH_3), 45.42 ($\underline{C}H_2CO$).

HRMS (ESI) *m*/*z*: $[M+H]^+$ calcd for $C_{17}H_{16}ClN_6O_3$, 387.0972; found, 387.0977 (error = 1.18 ppm).

4. Conclusions

This study demonstrates that rational modification of the AOH-1996 scaffold yields several promising candidates with potent anticancer activity in MCF-7 and U-87 cell lines. Structure–activity relationship (SAR) analysis revealed that derivatives incorporating electron-withdrawing or moderately lipophilic substituents—particularly on the amide side chain and triazole ring—significantly enhanced cytotoxic potency, while bulky or strongly electron-donating groups diminished activity. Notably, compounds **1f**, **2b**, **3b**, **3c**, and **3d** exhibited the most pronounced antiproliferative effects against the MCF-7 cell line with IC_{50} values ranging from 0.65 μM to 11.4 μM, and **3d** was also effective against the U-87 cell line, with an IC_{50} of 8.72 μM, highlighting the importance of specific aromatic and polar functionalities for optimal activity.

ADMET predictions indicated that most derivatives possessed favorable drug likeness and high intestinal absorption, with compounds **2b** and **3b** best satisfying stringent drug-likeness criteria. Several active compounds were predicted to inhibit P-glycoprotein, suggesting their potential to overcome multidrug resistance, although high plasma protein binding and rapid systemic elimination may limit the therapeutic index. Metabolic stability varied, with **1f**, **3b**, and **3c** showing lower CYP interaction probabilities and more favorable profiles, while **2b** and **3d** may be prone to rapid hepatic metabolism. All compounds presented moderate to high predicted toxicity, including potential cardiotoxicity, which emphasizes the need for careful optimization. It is noteworthy that the parental compound AOH1996 showed even higher predicted toxicity (including AMES mutagenicity and hepatotoxicity), indicating that the structural modifications in the derivatives may have

partially mitigated inherent liabilities. Taken together, these derivatives—particularly **2b** and **3b**—represent promising lead scaffolds for further preclinical development, with the understanding that future studies should focus on structural optimization or formulation strategies to overcome ADMET-related limitations while retaining antiproliferative activity. Collectively, these findings align with recent advances in naphthalene- and 2-quinolone-based PCNA-targeting anticancer agents, where fine-tuning of electronic and lipophilic properties is critical for maximizing potency and selectivity [22].

The most promising analogs—particularly **2b** and **3b**—combined strong antiproliferative activity with acceptable ADMET profiles, supporting their prioritization for further preclinical evaluation as potential compounds in cancer therapy.

Supplementary Materials: The following supporting information can be downloaded at: https://www.mdpi.com/article/10.3390/molecules31050862/s1, NMR spectra, GC/MS reports and methods.

Author Contributions: Conceptualization, M.J. and A.D.; methodology, S.J. and A.J.; validation, M.J., A.D., and D.S.; formal analysis, D.S.; investigation, S.J. and A.J.; resources, D.S.; data curation, A.J. and S.J.; writing—original draft preparation, S.J. and A.J.; writing—review and editing, S.J. and A.J.; visualization, S.J. and A.J.; supervision, M.J. and D.S. All authors have read and agreed to the published version of the manuscript.

Funding: This research received no external funding.

Institutional Review Board Statement: Not applicable.

Informed Consent Statement: Not applicable.

Data Availability Statement: Data are contained within the article or Supplementary Material.

Acknowledgments: The authors are grateful to Ona Adomėnienė for providing high quality substituted phenylacetylenes for this project.

Conflicts of Interest: The authors declare no conflicts of interest.

Abbreviations

The following abbreviations are used in this manuscript:

ADMET	Absorption, Distribution, Metabolism, Excretion, and Toxicity
APIM	AlkB homolog 2 PCNA-interacting motif
BBB	Blood–brain barrier
C_{Ar}	Aromatic carbon
CYP	Cytochrome P450 (drug-metabolizing enzymes)
DCM	Dichloromethane
DMEM	Dulbecco's modified Eagle medium
DMSO	Dimethyl sulfoxide
FBS	Fetal bovine serum
FDAMDD	FDA maximum recommended daily dose
H_{Ar}	Proton attached to aromatic carbon
hERG	Human ether-à-go-go-related gene potassium channel
H_{HAr}	Proton attached to heteroaromatic carbon
HIA	Human intestinal absorption
HLM	Human liver microsomal
MTT	3-(4,5-Dimethylthiazol-2-yl)-2,5-diphenyltetrazolium bromide
PARP1	Poly(ADP-ribose) polymerase 1
PCNA	Proliferating cell nuclear antigen
P-gp	P-Glycoprotein

PIP-box	PCNA-interacting protein box (short peptide motif that binds PCNA)
PPB	Plasma protein binding
SAR	Structure–activity relationship
TEA	Triethylamine
TLS	Translesion synthesis
VDss	Volume of distribution at steady state

References

1. Strzalka, W.; Ziemienowicz, A. Proliferating Cell Nuclear Antigen (PCNA): A Key Factor in DNA Replication and Cell Cycle Regulation. *Ann. Bot.* **2010**, *107*, 1127–1140. [CrossRef]
2. Wang, T.; Wang, Z. Targeting the "Undruggable": Small-Molecule Inhibitors of Proliferating Cell Nuclear Antigen (PCNA) in the Spotlight in Cancer Therapy. *J. Med. Chem.* **2025**, *68*, 2058–2088. [CrossRef] [PubMed]
3. Li, J.; Yong, T.; Chen, Y.; Zeng, T.; Zhang, K.; Wang, S.; Zhang, Y. Targeting PCNA/PARP1 Axis Inhibits the Malignant Progression of Hepatocellular Carcinoma. *Front. Pharmacol.* **2025**, *16*, 1571786. [CrossRef] [PubMed]
4. Lingeman, R.G.; Hickey, R.; Malkas, L.; Raoof, M.; Cawley, J. Abstract 3864: AOH1996: A Multi-Faceted Inhibitor of Metastasis via PCNA and Tumor Microenvironment Targeting. *Cancer Res.* **2025**, *85*, 3864. [CrossRef]
5. Gu, L.; Li, M.; Li, C.M.; Haratipour, P.; Lingeman, R.; Jossart, J.; Gutova, M.; Flores, L.; Hyde, C.; Kenjić, N.; et al. Small Molecule Targeting of Transcription-Replication Conflict for Selective Chemotherapy. *Cell Chem. Biol.* **2023**, *30*, 1235–1247.e6. [CrossRef]
6. Gu, L.; Lingeman, R.; Yakushijin, F.; Sun, E.; Cui, Q.; Chao, J.; Hu, W.; Li, H.; Hickey, R.J.; Stark, J.M.; et al. The Anticancer Activity of a First-in-Class Small-Molecule Targeting PCNA. *Clin. Cancer Res.* **2018**, *24*, 6053–6065. [CrossRef]
7. Wendel, S.O.; Snow, J.A.; Gu, L.; Banerjee, N.S.; Malkas, L.; Wallace, N.A. The Potential of PCNA Inhibition as a Therapeutic Strategy in Cervical Cancer. *J. Med. Virol.* **2023**, *95*, e29244. [CrossRef]
8. Kowalska, E.; Bartnicki, F.; Fujisawa, R.; Bonarek, P.; Hermanowicz, P.; Tsurimoto, T.; Muszynska, K.; Strzalka, W. Inhibition of DNA Replication by an Anti-PCNA Aptamer/PCNA Complex. *Nucleic Acids Res.* **2018**, *46*, 25–41. [CrossRef]
9. Hardebeck, S.; Jácobo Goebbels, N.; Michalski, C.; Schreiber, S.; Jose, J. Identification of a Potent PCNA-P15-Interaction Inhibitor by Autodisplay-Based Peptide Library Screening. *Microb. Biotechnol.* **2024**, *17*, e14471. [CrossRef]
10. Inoue, A.; Kikuchi, S.; Hishiki, A.; Shao, Y.; Heath, R.; Evison, B.J.; Actis, M.; Canman, C.E.; Hashimoto, H.; Fujii, N. A Small Molecule Inhibitor of Monoubiquitinated Proliferating Cell Nuclear Antigen (PCNA) Inhibits Repair of Interstrand DNA Cross-Link, Enhances DNA Double Strand Break, and Sensitizes Cancer Cells to Cisplatin. *J. Biol. Chem.* **2014**, *289*, 7109–7120. [CrossRef]
11. Waga, S.; Hannon, G.J.; Beach, D.; Stillman, B. The P21 Inhibitor of Cyclin-Dependent Kinases Controls DNA Replication by Interaction with PCNA. *Nature* **1994**, *369*, 574–578. [CrossRef] [PubMed]
12. Jossart, J.; Gu, L.; Haratipour, P.; Li, C.; Lingeman, R.; Hickey, R.; Malkas, L.; Perry, J.J. Abstract 6583: Developing a Selective Cancer Chemotherapy by Small Molecule-Based Targeting of PCNA Protein. *Cancer Res.* **2024**, *84*, 6583. [CrossRef]
13. Li, C.M.; Lingeman, R.G.; Gu, L.; Hickey, R.J.; Malkas, L.H. Abstract 4235: PCNA and Histone Deacetylase Targeted Inhibitors in Cutaneous T-Cell Lymphoma. *Cancer Res.* **2025**, *85*, 4235. [CrossRef]
14. Gu, L.; Hickey, R.J.; Malkas, L.H. Abstract 5645: Targeting Transcription-Replication Conflict for Selective Chemotherapy in Glioblastoma. *Cancer Res.* **2025**, *85*, 5645. [CrossRef]
15. Lingeman, R.G.; Hickey, R.J.; Malkas, L.H. Abstract 1875: Enhanced Lung Cancer Treatment Using AOH1996, a Potent PCNA Inhibitor. *Cancer Res.* **2024**, *84*, 1875. [CrossRef]
16. Gu, L.; Lingeman, R.; Li, M.; Hickey, R.; Liu, Y.; Malkas, L. Mechanistic Study of the Superior Anti-Cancer Properties of a First-in-Class Small Molecule Targeting PCNA. *J. Clin. Oncol.* **2019**, *37*, e14636. [CrossRef]
17. Haratipour, P.; Zangi, M.; Yaghoubi, M.; Gu, L.; Jossart, J.; Perry, J.J.; Malkas, L.H.; Hickey, R.J. Abstract 6989: Advancing AOH1996: Enhanced Anticancer Activity of next-Generation Small Molecule PCNA Inhibitors. *Cancer Res.* **2025**, *85*, 6989. [CrossRef]
18. Bartolowits, M.D.; Gast, J.M.; Hasler, A.J.; Cirrincione, A.M.; O'Connor, R.J.; Mahmoud, A.H.; Lill, M.A.; Davisson, V.J. Discovery of Inhibitors for Proliferating Cell Nuclear Antigen Using a Computational-Based Linked-Multiple-Fragment Screen. *ACS Omega* **2019**, *4*, 15181–15196. [CrossRef]
19. Liao, X.H.; Lu, D.L.; Wang, N.; Liu, L.Y.; Wang, Y.; Li, Y.Q.; Yan, T.B.; Sun, X.G.; Hu, P.; Zhang, T.C. Estrogen Receptor α Mediates Proliferation of Breast Cancer MCF-7 Cells via a P21/PCNA/E2F1-Dependent Pathway. *FEBS J.* **2014**, *281*, 927–942. [CrossRef]
20. Qin, H.; Gui, Y.; Ma, R.; Zhang, H.; Guo, Y.; Ye, Y.; Li, J.; Zhao, L.; Wang, Y. MiR-1258 Attenuates Tumorigenesis Through Targeting E2F1 to Inhibit PCNA and MMP2 Transcription in Glioblastoma. *Front. Oncol.* **2021**, *11*, 671144. [CrossRef]

21. Fu, L.; Shi, S.; Yi, J.; Wang, N.; He, Y.; Wu, Z.; Peng, J.; Deng, Y.; Wang, W.; Wu, C.; et al. ADMETlab 3.0: An Updated Comprehensive Online ADMET Prediction Platform Enhanced with Broader Coverage, Improved Performance, API Functionality and Decision Support. *Nucleic Acids Res.* **2024**, *52*, W422–W431. [CrossRef]
22. Tan, Z.; Wortman, M.; Dillehay, K.L.; Seibel, W.L.; Evelyn, C.R.; Smith, S.J.; Malkas, L.H.; Zheng, Y.; Lu, S.; Dong, Z. Small-Molecule Targeting of Proliferating Cell Nuclear Antigen Chromatin Association Inhibits Tumor Cell Growth. *Mol. Pharmacol.* **2012**, *81*, 811–819. [CrossRef]